Applied Surface Science 670 (2024) 160577

Contents lists available at ScienceDirect

Applied Surface Science

journal homepage: www.elsevier.com/locate/apsusc

Full length article

Unraveling oxygen-driven surface segregation dynamics in platinum-gold alloys

Andrea Berti [a], Matteo D'Alessio [a,1], Marco Bianchi [b,2], Luca Bignardi [a], Paolo Lacovig [c], Charlotte Sanders [d], Silvano Lizzit [c], Philip Hofmann [b], Antimo Marrazzo [a,3], Alessandro Baraldi [a,c,*]

[a] Department of Physics, University of Trieste, via Valerio 2, 34127, Trieste, Italy
[b] Department of Physics and Astronomy, Interdisciplinary Nanoscience Center (iNANO), Aarhus University, Ny Munkegade 120, 8000, Aarhus, Denmark
[c] Elettra Sincrotrone Trieste, Str. st. 14, km 163.5 in AREA Science Park, 34149, Trieste, Italy
[d] Central Laser Facility, STFC Rutherford Appleton Laboratory, Harwell, OX11 0QX, United Kingdom

ARTICLE INFO

Keywords:
Surface segregation
X-ray photoelectron spectroscopy
AuPt
Platinum
Density functional theory
Oxidation
Electrochemistry

ABSTRACT

In this study we use high-energy resolution and fast X-ray Photoelectron Spectroscopy (XPS) measurements combined with Density Functional Theory (DFT) calculations to investigate the interplay between surface segregation and bulk migration of Pt atoms on Au(111) in an oxygen environment. We demonstrate that the segregation of Pt atoms is significantly influenced by the oxygen partial pressure and identify a range of O_2 pressure where PtAu surface alloy formation is inhibited while promoting the formation of Au oxide. These findings are essential to understand the compositional changes in the bimetallic surface alloy, which could potentially lead to modifying the catalytic properties of PtAu up to catalyst deactivation. Our results offer a strategy to control Pt surface coverage on Au(111), a quantity that is of paramount relevance given the applications of PtAu alloys as catalysts in reactions such as the oxygen reduction reaction or the oxidation of methanol and carbon monoxide. Additionally, our findings indicate a method for controlling the composition and properties of the surface of PtAu catalysts through adjustments made during the formation of the PtAu alloy.

1. Introduction

Understanding the complex interplay between platinum and gold atoms in the PtAu alloy is crucial to unraveling the intricate mechanisms governing the physical and chemical properties of this bimetallic material. PtAu is a distinctive alloy that emerges as a versatile catalyst in electrochemistry [1–4] which has shown properties very relevant to current technological applications. Although its involvement in the context of various chemical reactions of primary importance in the field of electrocatalysis is unquestioned, a thorough understanding of its properties is challenged by the complexity of the atomistic mechanisms governing them, and that in many cases turn out to be still not fully understood. This is particularly relevant for the case of the Oxygen Reduction Reaction (ORR) [5,6] crucial in the technologies of fuel cells and metal-air batteries. Furthermore, PtAu is markedly assuming an important role in catalyzing the oxidation of key molecules such as CO [7,8] and methanol [8–10]. In general alloying with gold serves as a co-catalyst that enhances reactivity of platinum [11,12]. Amidst the array of potential alloying elements, gold emerges as an intriguing choice, due to its inherent stability. In contrast to platinum, gold is intrinsically inert, thereby augmenting the stability of the PtAu alloy [13]. Recent investigations have revealed trends that diverge based on different reaction dynamics [14–16] and showed the complex interplay of ligand, strain, and ensemble effects which can be understood through the shifts of the d-band centroid, a well-known indicator of chemical reactivity according to the Hammer-Nørskov model [17,18]. This intricate scenario extends not only to electronic properties but also to the structure of PtAu surface alloys. Density functional theory (DFT) calculations revealed that the imposition of tensile strain from the Au substrate in the PtAu surface alloys leads to an upward shift

* Corresponding author at: Department of Physics, University of Trieste, via Valerio 2, 34127, Trieste, Italy.
E-mail address: alessandro.baraldi@elettra.eu (A. Baraldi).
[1] Present Address: FIM Department, University of Modena & Reggio Emilia, 41125, Modena, Italy, and S3 Centre, Istituto Nanoscienze, CNR, 41125, Modena, Italy
[2] Present Address: Elettra Sincrotrone Trieste, AREA Science Park, 34149, Trieste, Italy
[3] Present Address: Scuola Internazionale Superiore di Studi Avanzati (SISSA), via Bonomea 265, 34136, Trieste, Italy

https://doi.org/10.1016/j.apsusc.2024.160577
Received 15 April 2024; Received in revised form 5 June 2024; Accepted 20 June 2024
Available online 26 June 2024

of the d-band center [19]. This shift enhances the reactivity of platinum, particularly for CO oxidation. However, a too large shift can be detrimental to ORR due to intensified interactions with reaction intermediates species, such as OH, resulting in the passivation of active sites [20]. Nevertheless, ensemble and ligand effects from neighboring Au atoms can counterbalance this, further enhancing surface reactivity [21,22]. Furthermore, the coordination states of Pt atoms increase the complexity of the system, in particular, low-coordinate atomic sites have higher d-band shifts and thus stronger metal-molecule interactions [23,24]. This complexity amplifies in the regime of submonolayer surface coverages, where the interplay of ligand, strain, and ensemble effects becomes more pronounced.

Within this intricate scenario, two overarching observations arise [15,25]. First, Au-rich PtAu alloys exhibit larger d-band shifts, strengthening Pt interaction with adsorbed molecules, thus bolstering reactivity for CO, ethylene, and methanol oxidation. This, however, comes at the cost of increased density of OH adsorbed species, which negatively impacts ORR. Conversely, Pt-rich PtAu alloys exhibit smaller d-band shifts, amplifying the kinetics of O_2 reduction and consequently enhancing ORR on the Pt surface atoms. For this reason, the process of surface segregation assumes a role of utmost importance since the miscibility of these two elements is crucial in shaping the desired catalytic properties. Nonetheless, the intrinsic dynamical nature of this process makes the investigation of this system even more challenging.

Although the segregation problem of Pt and Au on the PtAu catalyst is known since many years [7], an in-depth spectroscopic investigation is still missing so far and there is not a clear trend in the literature. Over the several experiments performed on different PtAu systems, there are works [26,27] which show intriguing results, but do not discuss the complex intermixing of Pt and Au. On the other hand, many other works report the importance of the bimetallic alloy composition [5,28–30], which is ruled by the segregation mechanisms. However, the comparison between ideal models of interface PtAu structures versus the most practical catalyst surfaces is still challenging. This is mainly due to the intricate surface segregation processes that can lead in many cases to deactivation towards longer times, changing the bimetallic surface alloy composition [30]. Over time, Au segregation can lead the surface alloy to become a pure Au or highly Au-enriched surface, compromising the reactivity and catalyst stability. For instance, in the context of ORR, the natural tendency to form an Au-enriched surface alloy [31] results in detrimental effects over time [32]. The control of Pt coverage is clearly of both fundamental and practical importance for optimizing the performance through enhanced reactivity and stability. One of the primary strategies to counter this challenge is the exploitation of adsorbate-induced Pt segregation, similarly to what was observed for other bimetallic alloys [33]. More specifically oxygen's affinity for platinum atoms in the PtAu system offers a means to reverse this natural detrimental tendency [32,34,35].

The study we present herein focuses on understanding the influence of oxygen in the segregation of Pt atoms at the PtAu interface and devising a strategy to control Pt surface coverage on Au(111). To explore the intricacies of the evolution of the surface stoichiometry with time, temperature, adsorbate coverages, and oxidation states we used a combined approach based on high-resolution fast XPS measurements [36] and DFT calculations. Our investigation performed on the Pt deposition on Au(111) represents an additional contribution on understanding the intricacies of the not completely understood segregation processes beyond this complex system.

2. Experimental and computational methods

2.1. Experimental methods

All measurements were carried out at the SuperESCA beamline [36,37] of the Elettra synchrotron radiation facility (Trieste, Italy). The ultra-high vacuum (UHV) system (base pressure $< 1 \times 10^{-10}$ mbar) is equipped with a sputter ion gun for sample cleaning, a mass spectrometer, low-energy electron diffraction (LEED) optics, and a SPECS PHOIBOS 150 hemispherical electron energy analyzer with a delay line detector. The Au(111) single crystal was cleaned in UHV conditions by repeated cycles of Ar^+ sputtering (E = 1.5 keV) and annealing to 920 K. The annealing and cooling rate was 1 K/s. The sample cleanliness and ordering were verified by LEED and X-ray photoelectron spectroscopy (XPS). The measurements reported in this work were also performed in UHV conditions. The Pt was evaporated from a high purity (99.995%) Pt wire (0.25 mm) resistively heated, with the sample kept at room temperature (RT). The evaporation rate was set between 0.15 and 0.40 ML/h. 1 ML corresponds to the surface density of the Au atoms in the Au(111) surface, i.e., to 1.39×10^{15} atoms/cm^2. It is important to note that the coverage of intercalated Pt atoms is calculated solely by considering the corresponding photoemission intensity, without correction for the electron mean free path (EMFP). High-energy resolution XPS and fast XPS of Au and Pt $4f_{7/2}$ core level spectra were acquired with a photon energy of 180 eV and an overall energy resolution of 50 meV. Analogously, the O 1s core-level spectra were collected using photon energies of 650 eV. All the spectra were measured in the normal emission geometry and the core-electron binding energy (BE) is referenced to the sample Fermi level, acquired after each core level spectrum. The peak-fit analysis was carried out using a combination of Doniach–Sunjic (DS) [38] profiles convoluted with a Gaussian. The lineshape parameters are the Lorentzian width (Γ), the Anderson singularity index (α), and the Gaussian width (G), the latter accounting for experimental and inhomogeneous broadening. A linear background was subtracted from the core level photoemission signal.

2.2. Computational methods

DFT and nudged elastic band (NEB) calculations were carried out with the Quantum ESPRESSO [39–41] distribution, using the Perdew–Burke–Ernzerhof (PBE) functional [42] and pseudopotentials from the SSSP efficiency library v.1.1.2 [43–46]. Au and Pt lattice parameters were obtained through a fit of the Birch–Murnaghan equation of state on DFT total energies, and correspond respectively to 4.15 Å and 3.97 Å, in agreement with previous computational results [43,47]. In all calculations, SSSP efficiency cutoffs [43] for plane wave kinetic energies were used, corresponding to 50 Ry and 400 Ry for wavefunctions and charge density respectively. Brillouin zone integrations were done with 5 × 5 × 1 Monkhorst–Pack k-point grid [48] centered at Gamma and 0.015 Ry of cold smearing [49]. The Coulomb interaction was truncated along the out-of-plane direction to avoid spurious interaction between periodic replicas of the system [50]. All surfaces for structural relaxations were modeled as four-layer 4 × 4 supercells with an out-of-plane lattice parameter of 37 Å, which guarantees 27 Å of vacuum between periodic replicas. The positions of atoms in the bottom two layers were fixed. Convergence thresholds of energy and forces in the structural optimization were respectively 10 meV and 5 meV/Å. Adsorption energies were calculated as

$$E_{\mathrm{ads},X} = E_{X+\mathrm{surf}} - E_X - E_{\mathrm{surf}} \quad (1)$$

where the total energies were obtained after structure optimization: $E_{X+\mathrm{surf}}$ is the energy of the surface with the adsorbate X, E_X is the energy of the isolated adsorbate and E_{surf} is the energy of the surface without the adsorbate. For the adsorption energies of Pt adatoms, E_X is the energy of one Pt atom in vacuum. For the structural relaxations involving H_2O, van der Waals interactions were included by means of the Grimme-D3 method [51]. For NEB calculations [52] the surfaces were modeled as four-layer 3 × 3 supercells. Atoms in the bottom two layers were fixed. The climbing image scheme [53] was employed in the determination of the minimum energy path, with a convergence threshold of 5 meV/Å on the forces orthogonal to the path. The initial and final states for the algorithm were chosen as highest adsorption energy configurations and the total path was discretized in 8 images (including the initial and final states).

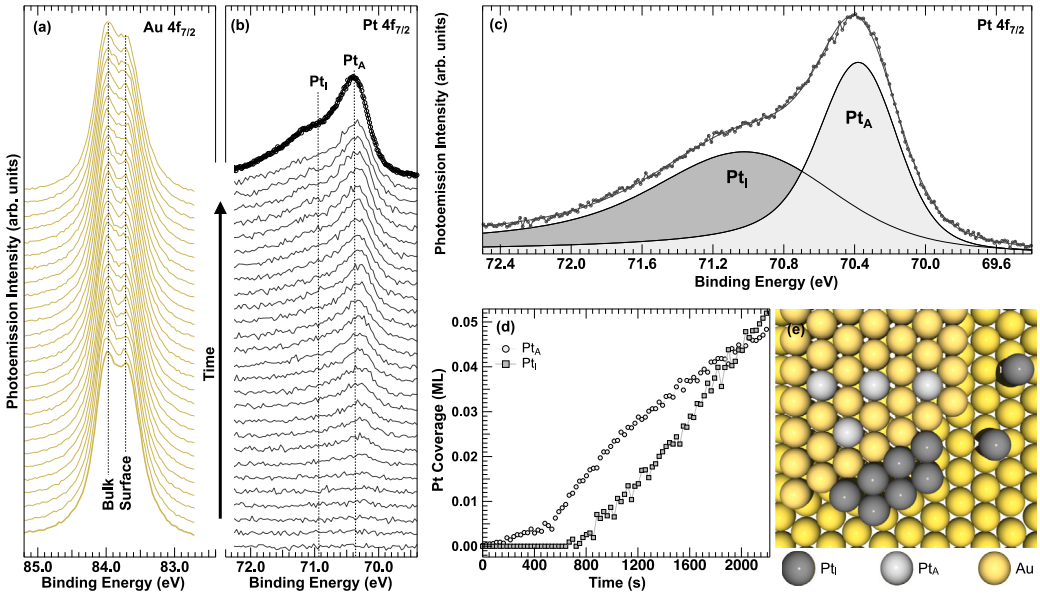

Fig. 1. Deposition of Pt atoms at room temperature. Evolution of the $4f_{7/2}$ (a) Au and (b) Pt core levels acquired with photons of energy $h\nu$ = 180 eV in real-time during the deposition process. For clarity, only 1 every 3 acquired spectra is shown, although in the analysis all the spectra have been considered. The acquisition time for Au and Pt were 10 s and 17 s, respectively. The first curve in bold of the Au spectral sequence represents the clean Au(111) spectrum. The Au bulk and surface components are highlighted, as well as the two components of the Pt spectra, namely Pt_A and Pt_I. (c) High-resolution Pt $4f_{7/2}$ core level spectrum acquired with the same photon energy at the end of the deposition, plotted with its spectral deconvolution. (d) Deposition curves for the Pt_A and Pt_I species. (e) Schematic drawing of the proposed bimetallic alloy growth mechanism.

3. Results and discussion

In Fig. 1(a) we display the Au $4f_{7/2}$ spectrum of the clean surface (first curve in bold), acquired at room temperature. This spectrum exhibits two components separated by approximately 0.32 eV, which we assign to bulk (83.95 eV) and surface atoms (83.63 eV), as previously reported [54].

The evolution of the $4f_{7/2}$ Au (Fig. 1(a)) and Pt (Fig. 1(b)) core levels was monitored during Pt deposition at room temperature, with a deposition rate of 0.15 ML/h. The Pt coverage obtained at the end of the deposition process is approximately 0.10 ML. Beyond a reduced overall intensity assigned to an attenuation effect on the photoelectrons due to the deposited platinum, in the Au $4f_{7/2}$ sequence we observe only a small reduction in the surface-to-bulk ratio, indicating that a fraction of the surface Au atoms interacts with or is substituted by Pt atoms. As expected, the Pt spectral sequence (Fig. 1(b)) shows an increasing photoemission signal, which is the result of two contributions, as shown at the end of the deposition, for the spectrum displayed in Fig. 1(c). The first contribution (Pt_A, BE=70.36 eV) arises since the early stages of deposition, while the second (Pt_I, BE=70.93 eV), starts growing after about 600 s since the beginning of the deposition and reaches the maximum intensity at the end of the process (see Fig. 1(d)). The deposition curves for the Pt_A and Pt_I species, shown in Fig. 1(d), exhibit specific trends, intersecting approximately 2000 s after the beginning of the deposition. While the curve associated to Pt_I continues to rise, the Pt_A component starts to slow down after about 1000 s. The spectral behavior of the Pt and Au core level spectra can be interpreted on the basis of the previous observations by Pedersen et al. [7] and Prieto et al. [55] for the PtAu surface, which are schematically described in Fig. 1(e). After the deposition of small amounts of Pt, single Pt adatoms begin to diffuse on the Au(111). However, when they reach steps or herringbone domain boundaries, which are known to act as barriers to diffusion, the PtAu alloy forms through an atomic exchange mechanism. The Au atoms displaced from the surface nucleate into 2D ad-islands, providing additional sites for Pt deposition. By increasing the amount of deposited Pt, similarly, this substitutional alloy continues to form on the newly formed 2D Au islands. Finally, only with further increase of the Pt coverage and the beginning of the nucleation of a second-layer, clean Pt islands start to form. We interpret the Pt_A component as caused by Pt atoms forming a surface bimetallic alloy with Au through substitution processes, as the measured Pt $4f_{7/2}$ core electron BE changes match those reported in the literature [56]. On the contrary, the Pt_I component is attributed to the formation of small Pt ad-islands above the Au(111) surface, as previously observed on other Au surfaces [55,57]. We suggest that the spectral broadening of this component is due to the different coordination numbers of the Pt atoms forming these islands. Such model accounts for the trend observed for the Pt_I component, which begins to appear with a certain delay with respect to Pt_A and then it becomes more intense along the Pt deposition process.

To interpret such spectroscopic data we performed DFT calculations of the total energies of the different configurations of Pt atoms on Au(111). The results of such analysis are reported in Fig. 2. The configuration of Pt embedded in the first layer of Au(111) surface (Fig. 2(b)) is energetically preferred compared to the configuration with an isolated Pt adatom on the clean Au(111) surface (Fig. 2(a)), since the total energy of the former is 0.84 eV lower. Additionally, our results suggest that the migration of Pt to the second layer of the surface (Fig. 2(c)) corresponds to a slightly more favored configuration, being its total energy 0.96 eV lower with respect to the Pt adatom on clean Au(111) (Fig. 2(a)). We also note that the configuration involving a Pt adatom bound to another Pt atom embedded in the first surface layer (Fig. 2(d)) is slightly preferred (E_{ads} = − 4.55 eV) when compared to that of an isolated adatom (Fig. 2(e), E_{ads} = − 4.36 eV). This result agrees with the observation that the nucleation process is favored only when overcoming a threshold coverage of Pt embedded in the first Au surface layer. Moreover, only Pt atoms in the first surface layer can act as nucleation seeds, since the adsorption energies of additional Pt adatoms are not significantly influenced by their proximity to Pt atoms in the second layer (E_{ads} = −4.31 eV when close and E_{ads} = −4.35 eV when far), as shown in Fig. S1 in the Supplementary Materials (SM). The near equivalence in energy between the two configurations in Fig. 2(b, c) suggest that Pt atoms are not confined exclusively to the surface of Au(111) but they might migrate, already at 300 K, towards sub-surface layers due to thermal excitation [55,58].

Such hypothesis was verified heating the sample after deposition at$T$ = 300 K. As shown in Fig. 3(a), the total photoemission intensity

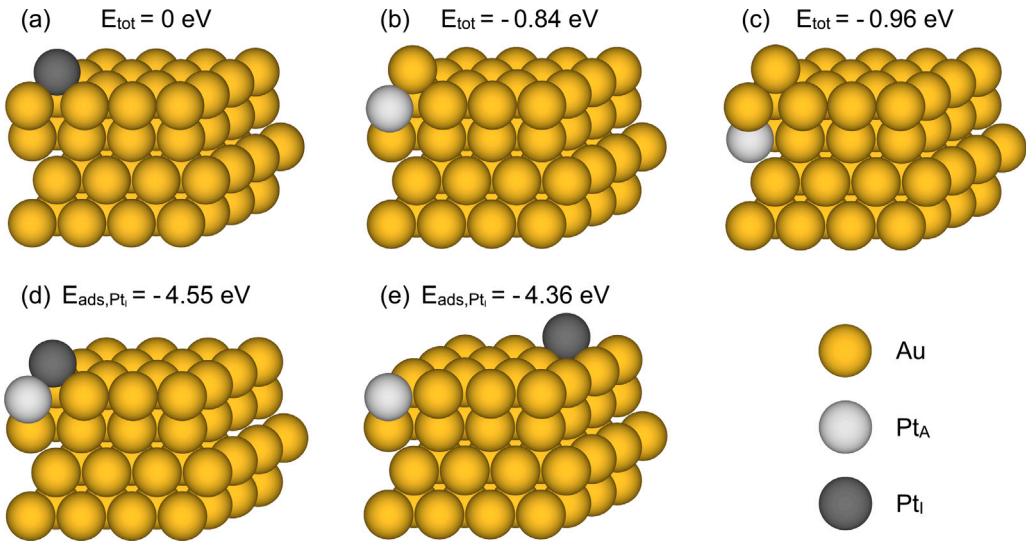

Fig. 2. DFT calculations of the total energy associated with the following configurations: (a) an isolated adatom on the clean Au(111) surface, (b) a Pt atom embedded in the first layer of the Au(111) surface, and (c) a Pt atom in the second layer of the surface. The zero of the total energy is set to the energy of structure (a), e.g. $E_{tot(b)} - E_{tot(a)} = -0.84$ eV . Adsorption energy of a Pt adatom bound to another Pt atom embedded in the first surface layer (d) and an isolated adatom (e).

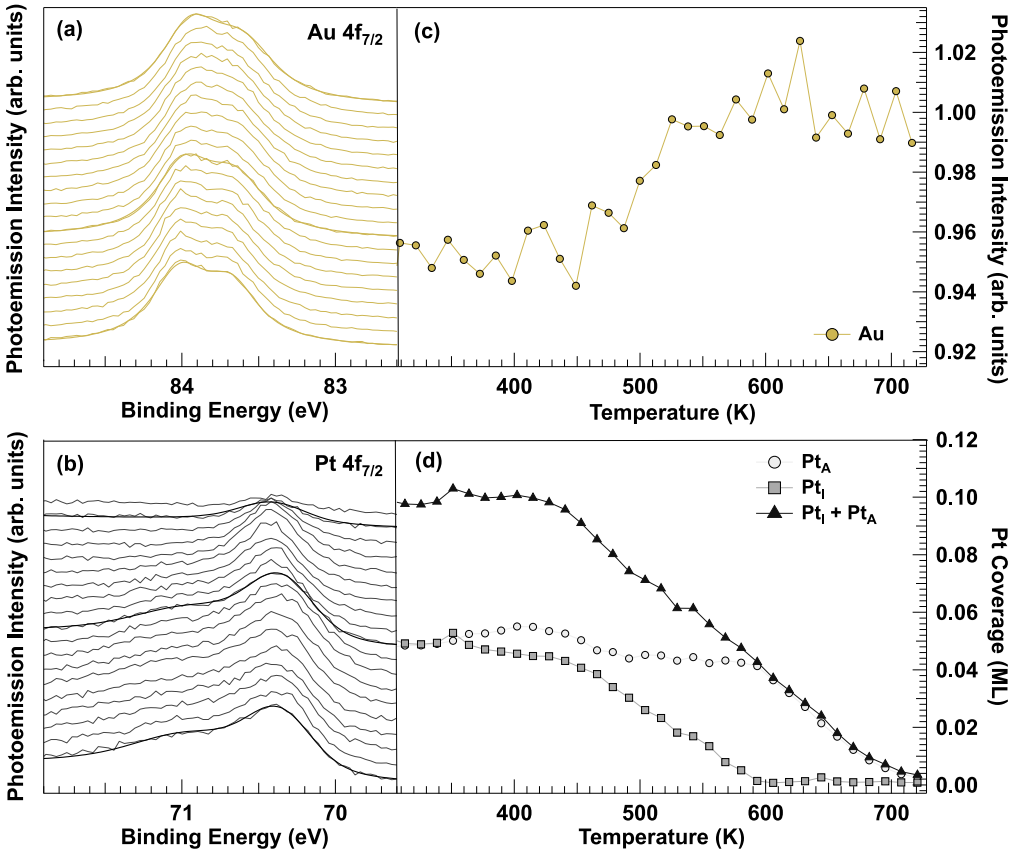

Fig. 3. Spectral sequences of $4f_{7/2}$ (a) Au and (b) Pt core levels acquired during annealing to 450 K in UHV (photon energy $h\nu$ = 180 eV). For clarity, only 1 every 2 acquired spectra is shown, although in the analysis all the spectra have been considered. The acquisition time for Au and Pt were 8 s and 17 s, respectively. The sample was previously grown by depositing Pt atoms at room temperature. (c) Evolution of the total (bulk and surface) photoemission intensity of Au. (d) Evolution of each spectral component of the Pt $4f_{7/2}$ core level and their sum.

of the Au $4f_{7/2}$ components clearly increases when sample temperature exceeds 450 K. On the contrary the overall Pt coverage decreases with increasing temperature, as illustrated in Fig. 3(b), in agreement with the increasing Au photoemission signal due to a weaker Pt attenuation effect. At the same time, the component previously associated with the islands Pt_I atop the surface starts decreasing significantly at a lower temperature compared to the alloy Pt_A component. Also, these trends strongly support the assignment of the different atomic species in agreement with the model discussed above. As the temperature increases, the atoms initially forming the Pt islands penetrate the first surface layer,

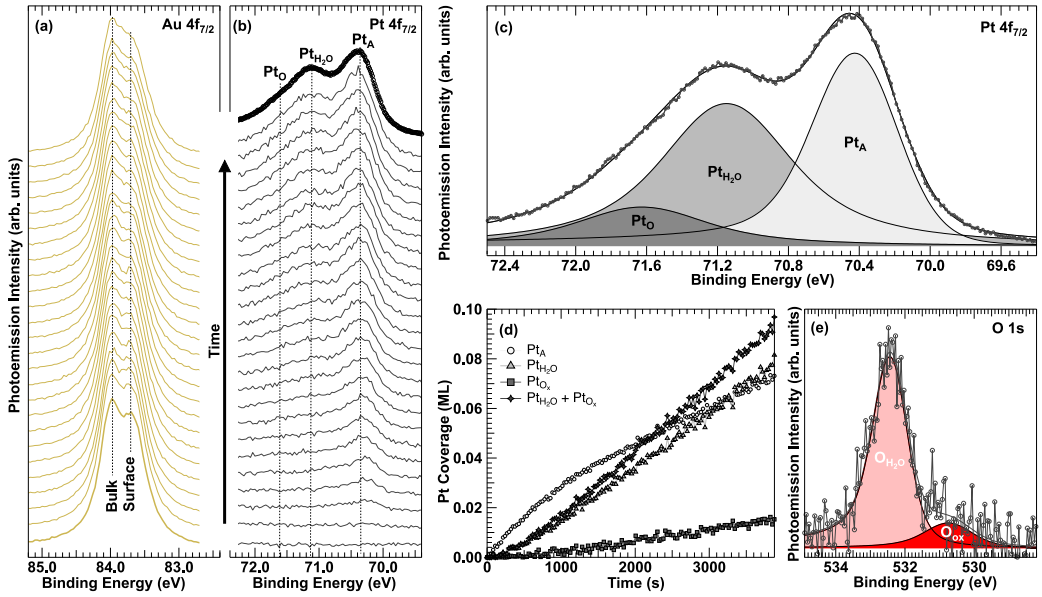

Fig. 4. Deposition of Pt atoms at room temperature under a O_2 partial pressure of 5×10^{-7} mbar. Evolution of the $4f_{7/2}$ (a) Au and (b) Pt core levels acquired with photons of energy $h\nu$ = 180 eV in real-time during the deposition process. For clarity, only 1 every 6 acquired spectra is shown, although in the analysis all the spectra have been considered. The acquisition time for Au and Pt were 10 s and 17 s, respectively. The first curve in bold of the Au spectral sequence represents the clean Au(111) spectrum. The Au bulk and surface components are highlighted, as well as the three components of the Pt spectra, namely Pt_A, Pt_{H_2O} and Pt_O. (c) High-resolution Pt $4f_{7/2}$ core level spectrum acquired with the same photon energy at the end of the deposition, plotted with its spectral deconvolution. (d) deposition curves for the Pt_A, Pt_{H_2O}, Pt_O, and Pt_{H_2O} + Pt_O species. (e) O 1s spectrum acquired at the end of the growth procedure with its spectral components (photon energy $h\nu$ = 650 eV).

leading to a reduced surface Pt coverage. Such Pt atoms form an alloy, analogously to the previously explained alloying mechanism. Interestingly, the intensity of the Pt_A component remains almost constant up to about 600 K. This behavior can be explained by considering that the atoms previously present in the first surface layer can diffuse into the bulk of the Au crystal, leaving space for the incoming Pt from the islands. If the Pt_I islands are present on the surface, these two flows balance each other leading to a Pt_A component almost unchanged. However, when the coverage of Pt_I atoms is extremely small, also the component associated with the alloy begins to decrease.

To exploit the adsorbate-induced effects on the mechanism of Pt surface segregation we repeated the growth procedure, but in an oxygen-rich environment. We deposited Pt atoms (same rate and temperature conditions) under a O_2 partial pressure of 5×10^{-7} mbar, for a total Pt coverage of 0.17 ML. The growth process was monitored by acquiring both the $4f_{7/2}$ core levels spectra of Au and Pt (see Fig. 4(a) and (b)). Concerning the Au, the observations closely align with those of the growth without oxygen, i.e., minor spectral variations were observed in the spectrum (see Fig. 4(a)), mainly related to the attenuation effect of the deposited platinum on the photoemission signal and the interaction involving a fraction of Au surface covered with Pt atoms.

At the same time, the Pt spectral sequence, shown in Fig. 4(b), exhibits the growth of three components at BEs of 70.36, 71.15, and 71.63 eV, as evident by the last spectrum of the series shown in Fig. 4(c). The Pt coverage evolution (Fig. 4(d)) shows that the lower BE component (Pt_A), associated with the surface alloy formation, once again is the first to grow in intensity. Markedly, the behavior of both the Pt_A component and the sum of the other two peaks, is very similar to the one obtained in the growth without oxygen, shown in Fig. 1(d), resulting in an intersection of the curves, also in this case, at approximately 2000 s. This result suggests that the growth mechanism remains almost the same, besides the appearance of new core level components at higher BEs. For a better understanding of the system, it is useful to discuss the behavior of the O 1s spectrum (see Fig. 4(e)), which clearly shows a component (O_{H_2O}) at 532.39 eV. This value is too high to be associated with atomic oxygen on Pt [59–61]; instead, it is more likely ascribable to the presence of H_2O/hydrated O:H_2O complexes [62–64]. As previously observed, the presence of H_2O on a Pt(111) surface results in the appearance of a Pt $4f_{7/2}$ component at about 71 eV [65,66], i.e., very close to the 71.15 eV value measured in our experiment. This component (Pt_{H_2O}) may arise from Pt islands partially covered with H_2O molecules, the latter produced as an unwanted species because of the O_2 reaction with hydrogen on the inner walls of the UHV chamber. We indeed notice that an O_2 pressure in the 10^{-7} mbar range results in a growth of the partial pressure of H_2O in the 3×10^{-10} mbar range.

The third $4f_{7/2}$ component (Pt_O) at BE=71.63 eV can be ascribed to the presence of Pt atoms with higher oxidation state. Such outcome agrees with the presence of a precursor oxidation state for the formation of surface oxides, as reported by previous experiments and theoretical calculations in the case of Pt single crystal surfaces [67,68]. Since this oxide generally forms along Pt crystal steps [69–71], we speculate that the Pt_O component may be related to the formation of oxide along the edges of the Pt islands. This interpretation is supported by the analysis of the O 1s spectrum acquired at the end of the process (see Fig. 4(e)) that, beside then O_{H_2O} component, shows an additional low intensity peak (O_{ox}) at 530.69 eV, indicative of the presence of Pt oxide [72,73]. The low intensity of both $4f_{7/2}$ Pt_O component and 1s O_{ox} oxygen peak thus suggest that the formation of Pt oxide is clearly hindered at the specific growth condition we have employed.

As a background pressure of oxygen of 5×10^{-7} mbar did not alter the mechanism or growth rate of the surface alloy we decided to investigate the evolution of this system employing even higher O_2 partial pressures. In Fig. 5, we show the data acquired during Pt deposition (same rate and temperature conditions as before) performed under a partial pressure of O_2 equal to 5×10^{-6} mbar, i.e., an order of magnitude larger than in the previous experiment, for a total Pt coverage of 0.19 ML. This growth leads to the appearance of three components in the Pt $4f_{7/2}$ spectra with BE=70.45, 71.17, and 71.70 eV (see Fig. 5(b) and (c)). These values are very close to those found in the lower oxygen pressure deposition and for this reason we attribute them to the same species, namely PtAu alloy (Pt_A), Pt islands bonded to H_2O (Pt_{H_2O}), and precursor oxidation state (Pt_O). However, a crucial difference arising from this growth lies in the spectral weight related to the individual

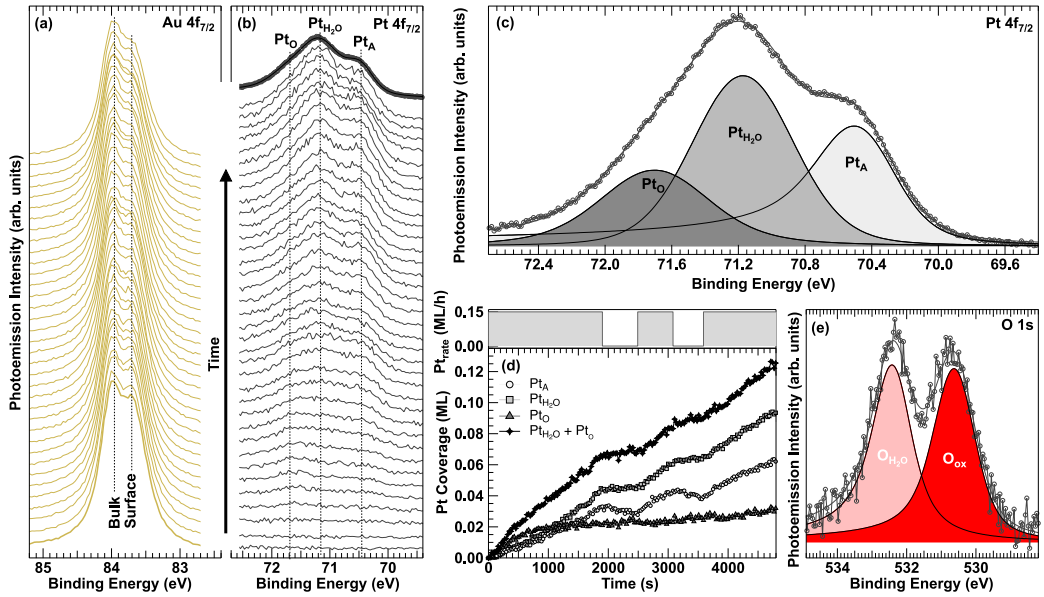

Fig. 5. Deposition of Pt atoms at room temperature under a O_2 partial pressure of 5×10^{-6} mbar. Evolution of the $4f_{7/2}$ (a) Au and (b) Pt core levels acquired with photons of energy $h\nu$ = 180 eV in real-time during the deposition process. For clarity, only 1 every 6 acquired spectra is shown, although in the analysis all the spectra have been considered. The acquisition time for Au and Pt were 10 s and 17 s, respectively. The first curve in bold of the Au spectral sequence represents the clean Au(111) spectrum. The Au bulk and surface components are highlighted, as well as the three components of the Pt spectra, namely Pt_A, Pt_{H_2O} and Pt_O. (c) High-resolution Pt $4f_{7/2}$ core level spectrum acquired with the same photon energy at the end of the deposition, plotted with its spectral deconvolution. (d) deposition curves for the Pt_A, Pt_{H_2O}, Pt_O, and Pt_{H_2O} + Pt_O species. The top part of the panel shows the profile of the Pt deposition rate during the growth, highlighting the two regions where the Pt deposition was stopped while leaving the system in a O_2 environment. (e) O 1s spectrum acquired at the end of the growth procedure with its spectral components (photon energy $h\nu$ = 650 eV).

components, which can be appreciated by observing the large increase in the population of atoms with a higher oxidation state.

Even more peculiar are the trends observed for the different Pt species, reported in Fig. 5(d). Firstly, it is worth to highlight how the alloy component, at this increased O_2 pressure, forms in quite smaller amount compared to previous depositions. Now, the growth rate of overall Pt atoms located above the surface (Pt_O+Pt_{H_2O}, black) and the one of Pt_A (light gray) differ from what was observed before. At the beginning they grow almost in parallel, but then the Pt above the surface proceeds faster. Hence, at this pressure, the oxygen has induced an enhanced surface segregation of Pt atoms, as previously supposed [5,32,34]. To support these spectroscopic results, we performed DFT calculations to determine the adsorption and total energies for various configurations of atomic oxygen adsorbed onto Pt atoms on Au(111). The outcomes are presented in Fig. S2 of the SM. In detail, the oxygen atom adsorbs on Pt embedded in the first layer of Au(111) surface with E_{ads} = − 3.56 eV. This value decreases to − 3.17 eV when the oxygen absorption occurs on the structure with the Pt atom in the second layer of the surface. Additionally, the first layer configuration is also slightly more preferred, being its total energy 0.13 eV lower with respect to the second one, unlike the result we obtained for Pt only (Fig. 2). Therefore, our results agree that oxygen can inhibit the migration of Pt atoms towards sub-surface layers. This outcome is not surprising, as it is known that the oxygen's affinity with Pt is greater than with Au [32,34,35]. Additionally, it is plausible to think that as the density of Pt in the first layer increases, local configurations where oxygen is bonded to more than one Pt atom may form. Such feature favors the Pt exchange process from the sub-surface to the first surface layer. To further investigate this effect, we monitored the evolution of the different species when Pt deposition is stopped while leaving the system in a O_2 background. The stops of the Pt exposure are highlighted by the profile of the Pt deposition rate shown in the top part of Fig. 5(d). The result is a clear decrease in the alloy component and an increase in the population of Pt atoms above the surface of Au(111). Moreover, the O 1s spectrum in Fig. 5(e) shows two components at BE=532.38 eV (O_{H_2O}) and 530.59 eV (O_{ox}), analogously to the values reported for the lower pressure growth. Nevertheless, in this case, the O_{ox} component associated with atomic oxygen is comparable in intensity to the O_{H_2O} component. The fact that the increased intensity of the precursor state in the Pt $4f_{7/2}$ spectrum goes along with an increase in the intensity of the atomic oxygen component further strengthens the previous species assignment. It might seem contradictory to think that certain Pt species bind to water while others only to oxygen. However, as reported in previous studies, the presence of extended and stable layers of chemisorbed oxygen can inhibit the adsorption of H_2O and similar molecules [74]. To strengthen this hypothesis, we calculated the adsorption energies of water on a ML of Pt on Au(111) both without and with oxygen atoms forming the well-known p(2x2) adlayer [75]. By comparing our results (see Fig. S3 in the SM) we found that the adsorption energy of H_2O on the bare Pt ML (E_{ads} = − 0.66 eV) is halved when the surface is covered with oxygen (E_{ads} = − 0.32 eV). Therefore, it is reasonable to expect that this oxide might show a more ordered and stable structure, inhibiting the adsorption of water or hydrated complexes in general. Moreover, it is reasonable that the increased presence of this ordered O-rich region along the edges might also partially inhibit the H_2O adsorption in its vicinity, possibly even in specific areas of the islands. This latter assumption could better explain the observed ratio between the two components in the O 1s spectrum.

In summary, the results about deposition of Pt at room temperature and at a partial pressure of O_2 equal to 5×10^{-6} mbar clearly demonstrate the Pt surface segregation process induced by the presence of dissociated O_2 on Au(111). Using the information gathered from the highest-pressure growth experiment, we decided to further inhibit the formation of the alloy by employing a cyclic two-steps procedure. The first step consists of depositing Pt at a rate of 0.4 ML/h at room temperature under a O_2 partial pressure of 3×10^{-5} mbar. In the second step, the Pt deposition was stopped, and the sample was left under the same O_2 flux. Each of the two stages was arbitrarily set to last for 300 s. The number of cycles define the final Pt coverage. In our experiment the total Pt coverage was 0.36 ML. Because of the much higher O_2 pressure employed for this set of measurements, we could not monitor the evolution of the $4f_{7/2}$ Pt and Au core levels in real time as before. Therefore, we decided to divide the entire growth into three subsequent phases, as shown in Fig. 6. At the end of each

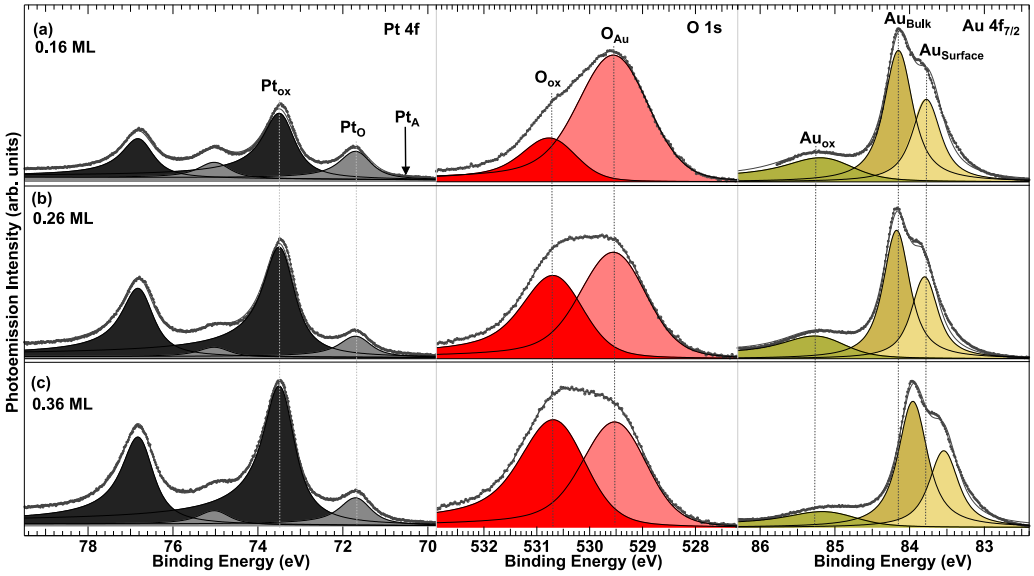

Fig. 6. Growth procedure performed at room temperature by repeated cycles of Pt deposition under a O_2 partial pressure of 3×10^{-5} mbar and subsequent exposure to O_2 only. High resolution $4f_{7/2}$ spectra of Pt and Au (photon energy $h\nu$ = 180 eV), and O 1s (photon energy $h\nu$ = 650 eV) core levels were acquired at three different stages of the experiment. In detail, the spectra plotted with their spectral decomposition refer to a Pt coverage of (a) 0.16 ML, (b) 0.26 ML, and (c) 0.36 ML.

phase, high resolution $4f_{7/2}$ spectra of Pt and Au, and O 1s core levels were acquired. Concerning the Pt $4f_{7/2}$ core levels, Fig. 6(a), only two distinct components are now evident at 71.67 and 73.45 eV. The first important observation is the complete absence of the Pt_A component associated with the alloy formation. These results indicate that the new procedure entirely inhibits the formation of the bimetallic alloy, thanks to the enhanced surface segregation of Pt induced by the higher oxygen pressure. The lower BE component (Pt_O) agrees once more with the presence of a precursor state to a surface oxide. Notably, in this case, a component (Pt_{ox}) appears for the first time at even higher BE (73.45 eV). This Pt_{ox} component is a fingerprint of the PtO_2 formation, as discussed in previous studies [67,76]. Nonetheless, the Pt_O component has not completely vanished, thus suggesting that a precursor state may still be localized along the edges of these oxide islands.

The behavior of the Au $4f_{7/2}$ spectra is quite remarkable: we have recorded the appearance of an additional component (Au_{ox}) with respect to clean gold, located at 85.03 eV (see Fig. 6(c)), which can be assigned to oxidized gold on the crystal surface [77–79]. This result is quite surprising as is well known that gold does not oxidize in the presence of O_2 at room temperature and atmospheric pressure. Therefore, the presence of Au atoms in high oxidation state is associated to the dissociation of molecular O_2 promoted by the Pt atoms on Au(111). The largely enhanced dissociation probability of O_2 is confirmed by the very low dissociation barrier (0.04 eV, Fig. S4 in SM) of O_2 on a monolayer of Pt on Au(111) found in our DFT calculations. An additional insight comes from the calculation of the projected density of states for Pt 5d orbitals for the bulk, for the Pt(111) surface and for a Pt monolayer on a Au(111) surface, see Fig. S5 in the SM. In this latter configuration, a significant narrowing of the density of states can be observed, which can be measured using the band centroid parameter. This parameter is widely recognized as an indicator of chemical reactivity according to the Hammer-Nørskov model [17,18]. The values we obtained for the three different cases are – 2.46 eV, – 1.95 eV, and – 1.55 eV, respectively, corroborating the idea that the reactivity of surface Pt atoms is enhanced by local atomic coordination and, even more, by the formation of bonds with Au atoms, in agreement with previous observations by Gohda et al. [19].The question that may arise is why this Au_{ox} component is seen only in these experimental conditions. One explanation can be found in the O_2 dissociation barrier that can be influenced by the number and the local geometries of Pt atoms involved in the process. Indeed, we observed that the barrier of 1.70 eV (Fig. S6(a)) calculated for a single Pt adatom atop the Au surface decreases to 1.17 eV (Fig. S6(b)) in the case of a single Pt atom embedded on the first surface layer. Moreover, as mentioned before, when an extended Pt layer is formed on Au(111) the barrier can be easily overcome even at room temperature. The high oxygen pressure conditions and increased surface density of Pt promote the O_2 dissociation process, resulting in the generation of atomic oxygen. This atomic oxygen can also diffuse onto the surface of Au, affecting its oxidation state.

It is also interesting to focus the attention on the O 1s spectra, reported in Fig. 5(b), which show two components at 530.59 and 529.50 eV. In line with the earlier discussion about the inhibition of water formation due to the arrangement of stable oxygen species on platinum, the core level peak associated with water is no longer observed. As for the component at higher BE, it corresponds to the previously discussed precursor state. However, previous results indicate that the O 1s core level due to the precursor state and the one associated with PtO_2 are actually very similar in BE [80], which does not allow us to unambiguously distinguish them using our spectroscopic approach. The new component formed at lower BE (O_{Au}) is ascribable to atomic oxygen bound to Au [77–79]. The assignment of the O 1s components is strengthened by the behavior of Pt and Au $4f_{7/2}$, and O 1s components measured with increasing deposition time. The increasing trend of the O_{ox} is mirrored by the behavior of PtO_2, contrary to what take place for the O_{Au} and Au_{ox} signals that decrease. This last observation also allows us to conclude that the growth of Au_{ox} occurs on the surface of gold in between the Pt_{ox} islands and not beneath them.

4. Conclusions

Our experiments have revealed the critical role of kinetic exchange processes at the solid-surface interface during the oxidation of the PtAu alloy. Although in the past there have been several rigorous studies focusing on the properties of the PtAu alloy, few have quantitatively investigated the evolution of the surface chemical composition during segregation process. This aspect assumes utmost importance in determining the catalytic properties of the system. It is particularly crucial considering the potential exploitation of the fundamental role of oxygen in controlling the properties of the desired catalyst through adsorbate-induced surface segregation mechanisms.

We investigated the surface segregation mechanism in PtAu alloy by core level photoemission spectroscopy in combination with DFT calculations. The Pt deposition on Au(111) performed at room temperature leads to the alloy formation through an atomic exchange process, while a fraction of Pt atoms grow as small ad-islands above the surface. Upon annealing we observe that the alloy formation is not confined exclusively to the first atomic layer but Pt atoms might migrate towards sub-surface layers due to thermal excitation. We have highlighted how the adsorbate-induced Pt surface segregation process is strongly dependent on the oxygen environment. In particular, the complete inhibition of the alloy formation is achieved for Pt deposition under a O_2 partial pressure of the order of 10^{-5} mbar. Interestingly, under these conditions, the formation of Au oxide occurs in between the Pt ad-islands, caused by the dissociation of molecular O_2 promoted by Pt atoms. Future investigations on utilizing the oxygen mediated surface segregation process could allow for the engineering of controllable properties of PtAu catalysts.

CRediT authorship contribution statement

Andrea Berti: Writing – review & editing, Writing – original draft, Visualization, Investigation, Formal analysis, Data curation. **Matteo D'Alessio:** Writing – review & editing, Visualization, Validation, Investigation, Formal analysis. **Marco Bianchi:** Writing – original draft, Validation, Investigation. **Luca Bignardi:** Writing – review & editing, Validation, Investigation. **Paolo Lacovig:** Writing – review & editing, Validation, Investigation. **Charlotte Sanders:** Writing – review & editing, Validation, Investigation. **Silvano Lizzit:** Writing – review & editing, Validation, Methodology, Investigation. **Philip Hofmann:** Writing – original draft, Validation, Investigation. **Antimo Marrazzo:** Writing – review & editing, Validation, Methodology, Investigation, Formal analysis. **Alessandro Baraldi:** Writing – review & editing, Writing – original draft, Supervision, Investigation, Funding acquisition, Conceptualization.

Declaration of competing interest

The authors declare that they have no known competing financial interests or personal relationships that could have appeared to influence the work reported in this paper.

Data availability

No data was used for the research described in the article.

Acknowledgments

A.B. and L.B. gratefully acknowledge the financial support from the MUR-PRIN 2022 project n. 20222FXZ33 entitled "Materials modeling for energy storage applications". A.M. acknowledges support from the ICSC - Centro Nazionale di Ricerca in High Performance Computing, Big Data and Quantum Computing, funded by European Union - NextGenerationEU - PNRR, Missione 4 Componente 2 Investimento 1.4. A. Berti and M. D'A. acknowledge support from Collegio Universitario per le Scienze "Luciano Fonda". A.M. and M. D'A. acknowledge CINECA for simulation time on Marconi100, under the ISCRA initiative and CINECA-UniTS agreement, for the availability of high-performance computing resources and support.

Appendix A. Supplementary data

Supplementary material related to this article can be found online at https://doi.org/10.1016/j.apsusc.2024.160577.

References

[1] Q. Guan, C. Zhu, Y. Lin, E.I. Vovk, X. Zhou, Y. Yang, H. Yu, L. Cao, H. Wang, X. Zhang, et al., Bimetallic monolayer catalyst breaks the activity–selectivity trade-off on metal particle size for efficient chemoselective hydrogenations, Nat. Catal. 4 (2021) 840–849.
[2] G.-R. Zhang, D. Zhao, Y.-Y. Feng, B. Zhang, D.S. Su, G. Liu, B.-Q. Xu, Catalytic Pt-on-Au nanostructures: why Pt becomes more active on smaller Au particles, ACS Nano 6 (2012) 2226–2236.
[3] K.-Q. Sun, Y.-C. Hong, G.-R. Zhang, B.-Q. Xu, Synergy between Pt and Au in Pt-on-Au nanostructures for chemoselective hydrogenation catalysis, ACS Catal. 1 (2011) 1336–1346.
[4] J. Zhao, H. Yuan, G. Yang, Y. Liu, X. Qin, Z. Chen, C. Weng-Chon, L. Zhou, S. Fang, AuPt bimetallic nanoalloys supported on SBA-15: A superior catalyst for quinoline selective hydrogenation in water, Nano Res. (2022) 1–7.
[5] Y.-J. Deng, V. Tripkovic, J. Rossmeisl, M. Arenz, Oxygen reduction reaction on Pt overlayers deposited onto a gold film: ligand, strain, and ensemble effect, ACS Catal. 6 (2016) 671–676.
[6] M. Shao, A. Peles, K. Shoemaker, M. Gummalla, P.N. Njoki, J. Luo, C.-J. Zhong, Enhanced oxygen reduction activity of platinum monolayer on gold nanoparticles, J. Phys. Chem. Lett. 2 (2011) 67–72.
[7] M.Ø. Pedersen, S. Helveg, A. Ruban, I. Stensgaard, E. Lægsgaard, J.K. Nørskov, F. Besenbacher, How a gold substrate can increase the reactivity of a Pt overlayer, Surf. Sci. 426 (1999) 395–409.
[8] J. Suntivich, Z. Xu, C.E. Carlton, J. Kim, B. Han, S.W. Lee, N. Bonnet, N. Marzari, L.F. Allard, H.A. Gasteiger, et al., Surface composition tuning of Au–Pt bimetallic nanoparticles for enhanced carbon monoxide and methanol electro-oxidation, J. Am. Chem. Soc. 135 (2013) 7985–7991.
[9] J.-H. Choi, K.-W. Park, I.-S. Park, K. Kim, J.-S. Lee, Y.-E. Sung, A PtAu nanoparticle electrocatalyst for methanol electro-oxidation in direct methanol fuel cells, J. Electrochem. Soc. 153 (2006) A1812.
[10] J. Luo, P.N. Njoki, Y. Lin, D. Mott, Wang, C.-J. Zhong, Characterization of carbon-supported AuPt nanoparticles for electrocatalytic methanol oxidation reaction, Langmuir 22 (2006) 2892–2898.
[11] K. Kodama, R. Jinnouchi, N. Takahashi, H. Murata, Y. Morimoto, Activities and stabilities of Au-modified stepped-Pt single-crystal electrodes as model cathode catalysts in polymer electrolyte fuel cells, J. Am. Chem. Soc. 138 (2016) 4194–4200.
[12] A. Dorjgotov, Y. Jeon, J. Hwang, B. Ulziidelger, H.S. Kim, B. Han, Y.-G. Shul, Synthesis of durable small-sized bilayer Au@ Pt nanoparticles for high performance PEMFC catalysts, Electrochim. Acta 228 (2017) 389–397.
[13] B. Hammer, J.K. Nørskov, Why gold is the noblest of all the metals, Nature 376 (1995) 238–240.
[14] S. Yin, Y. Ding, Bimetallic PtAu electrocatalysts for the oxygen reduction reaction: challenges and opportunities, Dalton T. 49 (2020) 4189–4199.
[15] E. Irissou, F. Laplante, S. Garbarino, M. Chaker, D. Guay, Structural and electrochemical characterization of metastable PtAu bulk and surface alloys prepared by crossed-beam pulsed laser deposition, J. Phys. Chem. C 114 (2010) 2192–2199.
[16] X. Xie, V. Briega-Martos, R. Farris, M. Dopita, M. Vorokhta, T. Skala, I. Matolínová, K.M. Neyman, S. Cherevko, I. Khalakhan, Optimal Pt–Au alloying for efficient and stable oxygen reduction reaction catalysts, ACS Appl. Mater. Interfaces 15 (2022) 1192–1200.
[17] B. Hammer, J.K. Nørskov, Theory of adsorption and surface reactions, in: R.M. Lambert, G. Pacchioni (Eds.), Chemisorption and Reactivity on Supported Clusters and Thin Films: Towards an Understanding of Microscopic Processes in Catalysis, Springer Netherlands, Dordrecht, 1997, pp. 285–351.
[18] A. Ruban, B. Hammer, P. Stoltze, H.L. Skriver, J.K. Nørskov, Surface electronic structure and reactivity of transition and noble metals, J. Mol. Catal. A 115 (1997) 421–429.
[19] Y. Gohda, A. Groß, Structure–reactivity relationship for bimetallic electrodes: Pt overlayers and PtAu surface alloys on Au(111), J. Electroanal. Chem. 607 (2007) 47–53.
[20] J. Zhang, M.B. Vukmirovic, Y. Xu, M. Mavrikakis, R.R. Adzic, Controlling the catalytic activity of platinum-monolayer electrocatalysts for oxygen reduction with different substrates, Angew. Chem. - Int. Ed. 117 (2005) 2170–2173.
[21] F. Chang, S. Shan, V. Petkov, Z. Skeete, A. Lu, J. Ravid, J. Wu, J. Luo, G. Yu, Y. Ren, et al., Composition tunability and (111)-dominant facets of ultrathin platinum–gold alloy nanowires toward enhanced electrocatalysis, J. Am. Chem. Soc. 138 (2016) 12166–12175.
[22] H. Xin, A. Holewinski, S. Linic, Predictive structure–reactivity models for rapid screening of Pt-based multimetallic electrocatalysts for the oxygen reduction reaction, ACS Catal. 2 (2012) 12–16.
[23] H.-S. Su, X.-G. Zhang, J.-J. Sun, X. Jin, D.-Y. Wu, X.-B. Lian, J.-H. Zhong, B. Ren, Real-space observation of atomic site-specific electronic properties of a Pt nanoisland/Au(111) bimetallic surface by tip-enhanced Raman spectroscopy, Angew. Chem. - Int. Ed. 130 (2018) 13361–13365.
[24] L. Bianchettin, A. Baraldi, S. de Gironcoli, E. Vesselli, S. Lizzit, L. Petaccia, G. Comelli, R. Rosei, Core level shifts of undercoordinated Pt atoms, J. Chem. Phys. 128 (2008) 114706.

[25] A. Damjanovic, V. Brusić, Oxygen reduction at Pt-Au and Pd-Au alloy electrodes in acid solution, Electrochim. Acta 12 (1967) 1171–1184.
[26] M. Li, P. Liu, R.R. Adzic, Platinum monolayer electrocatalysts for anodic oxidation of alcohols, J. Phys. Chem. Lett. 3 (2012) 3480–3485.
[27] S.-E. Bae, D. Gokcen, P. Liu, P. Mohammadi, S.R. Brankovic, Size effects in monolayer catalysis—model study: Pt submonolayers on Au(111), Electrocatalysis 3 (2012) 203–210.
[28] D.Y. Chung, S. Park, H. Lee, H. Kim, Y.-H. Chung, J.M. Yoo, D. Ahn, S.-H. Yu, K.-S. Lee, M. Ahmadi, et al., Activity–stability relationship in Au@ Pt nanoparticles for electrocatalysis, ACS Energy Lett. 5 (2020) 2827–2834.
[29] B. Du, Tong, A coverage-dependent study of Pt spontaneously deposited onto Au and Ru surfaces: direct experimental evidence of the ensemble effect for methanol electro-oxidation on Pt, J. Phys. Chem. B 109 (2005) 17775–17780.
[30] S.H. Ahn, Y. Liu, T.P. Moffat, Ultrathin platinum films for methanol and formic acid oxidation: activity as a function of film thickness and coverage, ACS Catal. 5 (2015) 2124–2136.
[31] A. Ruban, H.L. Skriver, J.K. Nørskov, Surface segregation energies in transition-metal alloys, Phys. Rev. B 59 (1999) 15990.
[32] A. Dhouib, H. Guesmi, DFT study of the M segregation on MAu alloys (M=Ni, Pd, Pt) in presence of adsorbed oxygen O and O_2, Chem. Phys. Lett. 521 (2012) 98–103.
[33] A. Baraldi, D. Giacomello, L. Rumiz, M. Moretuzzo, S. Lizzit, F. Buatier de Mongeot, G. Paolucci, G. Comelli, R. Rosei, B.E. Nieuwenhuys, et al., Unexpected behavior of the surface composition of PtRh alloys during chemical reaction, J. Am. Chem. Soc. 127 (2005) 5671–5674.
[34] V. Tripkovic, H.A. Hansen, J. Rossmeisl, T. Vegge, First principles investigation of the activity of thin film Pt, Pd and Au surface alloys for oxygen reduction, Phys. Chem. Chem. Phys. 17 (2015) 11647–11657.
[35] B.L. Abrams, P.C. Vesborg, J.L. Bonde, T.F. Jaramillo, I. Chorkendorff, Dynamics of surface exchange reactions between Au and Pt for HER and HOR, J. Electrochem. Soc. 156 (2008) B273.
[36] A. Baraldi, G. Comelli, S. Lizzit, M. Kiskinova, G. Paolucci, Real-time X-ray photoelectron spectroscopy of surface reactions, Surf. Sci. Rep. 49 (2003) 169–224.
[37] A. Baraldi, M. Barnaba, B. Brena, D. Cocco, G. Comelli, S. Lizzit, G. Paolucci, R. Rosei, Time resolved core level photoemission experiments with synchrotron radiation, J. Electron Spectrosc. 76 (1995) 145–149.
[38] S. Doniach, M. Sunjic, Many-electron singularity in X-ray photoemission and X-ray line spectra from metals, J. Phys. C Solid State Phys. 3 (1970) 285.
[39] P. Giannozzi, S. Baroni, N. Bonini, M. Calandra, R. Car, C. Cavazzoni, D. Ceresoli, G.L. Chiarotti, M. Cococcioni, I. Dabo, et al., QUANTUM ESPRESSO: a modular and open-source software project for quantum simulations of materials, J. Phys.: Condens. Matter. 21 (2009) 395502.
[40] P. Giannozzi, O. Andreussi, T. Brumme, O. Bunau, M.B. Nardelli, M. Calandra, R. Car, C. Cavazzoni, D. Ceresoli, M. Cococcioni, et al., Advanced capabilities for materials modelling with quantum ESPRESSO, J. Phys.: Condens. Matter. 29 (2017) 465901.
[41] P. Giannozzi, O. Baseggio, P. Bonfà, D. Brunato, R. Car, I. Carnimeo, C. Cavazzoni, S. De Gironcoli, P. Delugas, F. Ferrari Ruffino, et al., Quantum ESPRESSO toward the exascale, J. Chem. Phys. 152 (2020).
[42] J.P. Perdew, K. Burke, M. Ernzerhof, Generalized gradient approximation made simple, Phys. Rev. Lett. 77 (1996) 3865.
[43] G. Prandini, A. Marrazzo, I.E. Castelli, N. Mounet, N. Marzari, Precision and efficiency in solid-state pseudopotential calculations, npj Comput. Mater. 4 (2018) 72.
[44] D. Hamann, Optimized norm-conserving Vanderbilt pseudopotentials, Phys. Rev. B 88 (2013) 085117.
[45] P.E. Blöchl, Projector augmented-wave method, Phys. Rev. B 50 (1994) 17953.
[46] D. Vanderbilt, Soft self-consistent pseudopotentials in a generalized eigenvalue formalism, Phys. Rev. B 41 (1990) 7892.
[47] P. Haas, F. Tran, P. Blaha, Calculation of the lattice constant of solids with semilocal functionals, Phys. Rev. B 79 (2009) 085104.
[48] H.J. Monkhorst, J.D. Pack, Special points for Brillouin-zone integrations, Phys. Rev. B 13 (1976) 5188.
[49] N. Marzari, D. Vanderbilt, A. De Vita, M. Payne, Thermal contraction and disordering of the Al(110) surface, Phys. Rev. Lett. 82 (1999) 3296.
[50] T. Sohier, M. Calandra, F. Mauri, Density functional perturbation theory for gated two-dimensional heterostructures: Theoretical developments and application to flexural phonons in graphene, Phys. Rev. B 96 (2017) 075448.
[51] S. Grimme, J. Antony, S. Ehrlich, H. Krieg, A consistent and accurate ab initio parametrization of density functional dispersion correction (DFT-D) for the 94 elements H-Pu, J. Chem. Phys. 132 (15) (2010).
[52] G. Henkelman, H. Jónsson, Improved tangent estimate in the nudged elastic band method for finding minimum energy paths and saddle points, J. Chem. Phys. 113 (22) (2000) 9978–9985.
[53] G. Henkelman, B.P. Uberuaga, H. Jónsson, A climbing image nudged elastic band method for finding saddle points and minimum energy paths, J. Chem. Phys. 113 (2000) 9901–9904.
[54] P. Heimann, J. Van der Veen, D. Eastman, Structure-dependent surface core level shifts for the Au(111), (100), and (110) surfaces, Solid State Commun. 38 (1981) 595–598.
[55] M.J. Prieto, E.A. Carbonio, S. Fatayer, R. Landers, A. De Siervo, Electronic and structural study of Pt-modified Au vicinal surfaces: a model system for Pt–Au catalysts, Phys. Chem. Chem. Phys. 16 (2014) 13329–13339.
[56] S.E. Hörnström, L. Johansson, A. Flodström, R. Nyholm, J. Schmidt-May, Surface and bulk core level binding energy shifts in Pt-Au alloys, Surf. Sci. 160 (1985) 561–570.
[57] M.J. Prieto, E.A. Carbonio, R. Landers, A. de Siervo, Promotion effect of platinum on gold's reactivity: A high-resolution photoelectron spectroscopy study, J. Phys. Chem. C 120 (2016) 10227–10236.
[58] A. Trembułowicz, A. Sabik, L. Jurczyszyn, Structural and electronic properties of Pt modified Au(100) surface, Sci. Rep. 12 (2022) 3859.
[59] M. Peuckert, H. Bonzel, Characterization of oxidized platinum surfaces by X-ray photoelectron spectroscopy, Surf. Sci. 145 (1984) 239–259.
[60] W. Ranke, Low temperature adsorption and condensation of O_2, H_2O and NO on Pt(111), studied by core level and valence band photoemission, Surf. Sci. 209 (1989) 57–76.
[61] M.A. Henderson, The interaction of water with solid surfaces: fundamental aspects revisited, Surf. Sci. Rep. 46 (2002) 1–308.
[62] M. Kiskinova, G. Pirug, H. Bonzel, Adsorption and decomposition of H_2O on a K-covered Pt(111) surface, Surf. Sci. 150 (1985) 319–338.
[63] S. Strbac, S. Petrovic, R. Vasilic, J. Kovac, A. Zalar, Z. Rakocevic, Carbon monoxide oxidation on Au(111) surface decorated by spontaneously deposited Pt, Electrochim. Acta 53 (2007) 998–1005.
[64] G.B. Fisher, J.L. Gland, The interaction of water with the Pt(111) surface, Surf. Sci. 94 (1980) 446–455.
[65] T. Schiros, L.-A. Näslund, K. Andersson, J. Gyllenpalm, G. Karlberg, M. Odelius, H. Ogasawara, L.G. Pettersson, A. Nilsson, Structure and bonding of the water-hydroxyl mixed phase on Pt(111), J. Phys. Chem. C 111 (2007) 15003–15012.
[66] H. Ogasawara, B. Brena, D. Nordlund, M. Nyberg, A. Pelmenschikov, L. Pettersson, A. Nilsson, Structure and bonding of water on Pt(111), Phys. Rev. Lett. 89 (2002) 276102.
[67] D. Miller, H. Öberg, S. Kaya, H.S. Casalongue, D. Friebel, T. Anniyev, H. Ogasawara, H. Bluhm, L.G. Pettersson, A. Nilsson, Oxidation of Pt(111) under near-ambient conditions, Phys. Rev. Lett. 107 (2011) 195502.
[68] J. Wang, W. Li, M. Borg, J. Gustafson, A. Mikkelsen, T. Pedersen, E. Lundgren, J. Weissenrieder, J. Klikovits, M. Schmid, et al., One-dimensional PtO_2 at Pt steps: formation and reaction with CO, Phys. Rev. Lett. 95 (2005) 256102.
[69] Z. Zhu, F. Tao, F. Zheng, R. Chang, Y. Li, L. Heinke, Z. Liu, M. Salmeron, G.A. Somorjai, Formation of nanometer-sized surface platinum oxide clusters on a stepped Pt(557) single crystal surface induced by oxygen: a high-pressure STM and ambient-pressure XPS study, Nano Lett. 12 (2012) 1491–1497.
[70] J. Bandlow, P. Kaghazchi, T. Jacob, C. Papp, B. Tränkenschuh, R. Streber, M. Lorenz, T. Fuhrmann, R. Denecke, H.-P. Steinrück, Oxidation of stepped Pt(111) studied by x-ray photoelectron spectroscopy and density functional theory, Phys. Rev. B 83 (2011) 174107.
[71] S. Günther, A. Scheibe, H. Bluhm, M. Haevecker, E. Kleimenov, A. Knop-Gericke, R. Schlögl, R. Imbihl, In situ X-ray photoelectron spectroscopy of catalytic ammonia oxidation over a Pt(533) surface, J. Phys. Chem. C 112 (2008) 15382–15393.
[72] C. Parkinson, M. Walker, C. McConville, Reaction of atomic oxygen with a Pt(111) surface: chemical and structural determination using XPS, CAICISS and LEED, Surf. Sci. 545 (2003) 19–33.
[73] C. Puglia, A. Nilsson, B. Hernnäs, O. Karis, P. Bennich, N. Mårtensson, Physisorbed, chemisorbed and dissociated O_2 on Pt(111) studied by different core level spectroscopy methods, Surf. Sci. 342 (1995) 119–133.
[74] R. Arrigo, M. Hävecker, M.E. Schuster, C. Ranjan, E. Stotz, A. Knop-Gericke, R. Schlögl, In situ study of the gas-phase electrolysis of water on platinum by NAP-XPS, Angew. Chem. - Int. Ed. 52 (2013) 11660–11664.
[75] K. Mortensen, C. Klink, F. Jensen, F. Besenbacher, I. Stensgaard, Adsorption position of oxygen on the Pt(111) surface, Surf. Sci. Lett. 220 (2–3) (1989) L701–L708.
[76] D.R. Butcher, M.E. Grass, Z. Zeng, F. Aksoy, H. Bluhm, W.-X. Li, B.S. Mun, G.A. Somorjai, Z. Liu, In situ oxidation study of Pt(110) and its interaction with CO, J. Am. Chem. Soc. 133 (2011) 20319–20325.
[77] A.Y. Klyushin, T.C. Rocha, M. Hävecker, A. Knop-Gericke, R. Schlögl, A near ambient pressure XPS study of Au oxidation, Phys. Chem. Chem. Phys. 16 (2014) 7881–7886.
[78] T. Yoshida, M. Okoshi, The patterned Au oxide layer formation on Au surfaces by F_2 laser irradiation under the atmospheric conditions, Surf. Interfaces 32 (2022) 102104.
[79] A. Stadnichenko, S. Koshcheev, A. Boronin, An XPS and TPD study of gold oxide films obtained by exposure to RF-activated oxygen, J. Struct. Chem. 56 (2015) 557–565.
[80] M.A. Van Spronsen, J.W. Frenken, I.M. Groot, Observing the oxidation of platinum, Nature Commun. 8 (2017) 429.